AIP | Journal of Applied Physics

Two-dimensional spatially periodic electron flow in various emission regimes

A Rokhlenko and J. L. Lebowitz

Citation: J. Appl. Phys. **107**, 103301 (2010); doi: 10.1063/1.3371261
View online: http://dx.doi.org/10.1063/1.3371261
View Table of Contents: http://jap.aip.org/resource/1/JAPIAU/v107/i10
Published by the American Institute of Physics.

Two-dimensional spatially periodic electron flow in various emission regimes

A Rokhlenko[a] and J. L. Lebowitz[b]
Department of Mathematics, Rutgers University Piscataway, New Jersey 08854-8019, USA

(Received 20 November 2009; accepted 24 February 2010; published online 20 May 2010)

We study the effects of cathode surface curvature on the space charge limited current emitted by a two-dimensional periodic array of field emitters. Each of these emitters has a shape described by a simple analytic function. Linear, quadratic, and Fowler–Nordheim current-field dependences of the cathode emissivity as well as the infinite emissivity Child–Langmuir model are considered. We develop a mathematical anzatz to capture the main features of the potential field structure of this system and supplement it with a set of correction functions with free parameters. A special least square procedure is used for an approximate solution of this nonlinear problem. We find that even a smooth curved cathode can yield significant spatial variations in the current density but for the cases considered it does not change substantially the total current (properly adjusted). When the cathode emissivity and/or the applied voltage are high enough the current density from the top of the cathode bump (where the curvature is maximal) exceeds the current density produced by a flat cathode with infinite emissivity placed at the same distance from the anode. An explanation of this effect is given. The spatial pattern of emission is determined almost solely by the cathode curvature no matter how strong the current is. © *2010 American Institute of Physics*. [doi:10.1063/1.3371261]

I. INTRODUCTION

Controlled electron flow is a basic component in numerous technological systems. In particular, it plays a very important role in field emission devices in which the electron flow can be effectively and rapidly controlled. These field emitters require strong electric fields E at the cathode surface to facilitate electron tunneling through a potential barrier.

The theoretical treatment of field emission is generally based on the well known Fowler–Nordheim (FN) equation for the current density J

$$J = QE^2 \exp(-P/E), \tag{1}$$

where Q and P depend on the cathode material and temperature. They are approximately independent of E when the electric field is not very strong but in strong fields the E-dependence of these parameters cannot be ignored because the top of the potential barrier is affected by the field. Equation (1) and its modifications are derived (see Refs. 1 and 2) on the basis of the quantum theory of electron tunneling and then reduced to the form in Eq. (1) by a weak field approximation (see some details in Sec. V). The real physical parameters of emitting materials are such that even practically strong electric fields (up to several kilovolt per micron) are in fact "weak" enough for this approach to be valid.

The exponential term in Eq. (1) makes the current extremely sensitive to even very small changes in the field strength at the cathode surface. A way to increase the field for a given applied voltage is by increasing the curvature of the emitting surface[3] and thus field emission cathodes in many systems are designed with various surface irregularities like sharp spikes.[4,5] While this yields high currents from the tips, the rest of the cathode surface emits only a small current. Therefore, to get a maximum total current one has to take into account not just the cathode bumps but the whole emitting surface. Optimization, therefore, requires a careful analysis of the full system.

In this work we study a simplified version of the above problem by considering a two-dimensional (2D) spatially periodic field emission system, which can be viewed as a model of a diode whose cathode has equidistant parallel ridges and the spacing between the electrodes is much smaller than the transverse dimensions. The periodicity allows us to simplify the problem by choosing a single cell, a "diode," where one can explore space charge effects for several emission laws including Eq. (1) over a wide range of cell parameters. We impose a very strong magnetic field in the Z-direction in Fig. 1 which means that emitted electrons all travel in this direction, i.e., normally to the mean electrode surfaces. This makes our computations simpler but, based on previous studies,[6] should not change the result drastically.

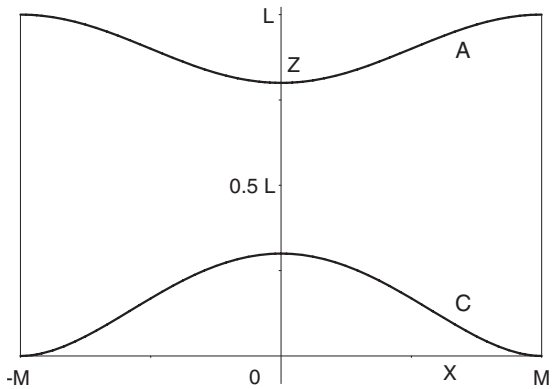

FIG. 1. Geometry of one chosen emission cell.

[a]Electronic mail: rokhlenk@math.rutgers.edu.
[b]Also at Department of Physics.

Our aim is to construct a flexible mathematical model of the potential inside the diode with adjustable free parameters chosen to obtain a self-consistent solution for both the current density and field distribution. The results provide information about the influence of the curvature of the emitting surface on the local and total currents.

To get more insight into the effect of cathode curvature on the current we consider first three idealized models of cathode emissivity using dimensionless quantities and equations: unlimited emission, which can be practically relevant in the case of thermionic emission, is discussed in Sec. III. In Sec. IV we consider the linear and quadratic current-field dependences. While these do not exist in reality they are easier to model and in addition they are exactly solvable in the flat diode, one-dimensional (1D) case. Their exploration suggests tendencies in the behavior of the current as a function of the emission law. Section V is devoted to the realistic FN emission model which is treated using the MKSA system to describe the current density profile and the current-voltage characteristics of our system as functions of the physical emitter parameters.

II. FORMULATION OF MODEL

We consider a model for the flow of charged particles in a very strong magnetic field in the Z-direction when both the cathode and anode have a simple periodic pattern of the same period but of a different shape generally. The cross section of one cell (a single period) of the flow in the $X-Z$ plane is shown in Fig. 1. The cathode and anode are marked by the letters C and A, respectively.

The cathode has infinite emissivity, as in the Child–Langmuir (CL) case,[7] or its emission satisfies some given law, like linear, quadratic or FN for the dependence[1,8] of the current density on the electric field normal to the cathode surface. Our goal is to develop efficient and straightforward calculations of the steady state currents for relatively simple 2D geometries, using only minimal approximations: some approximations are unavoidable for this very difficult nonlinear problem. This should provide useful checks on calculations for the design of devices which utilize strong currents of charged particles.

Let $\Phi(X,Z)$ and $\rho(X,Z)$ be the electric potential and electron number density in the cell, respectively. The electric current density J which, due to the strong magnetic field, depends only on X, is given by

$$J(X) = ev(X,Z)\rho(X,Z), \tag{2}$$

where $-e$ is the electron charge and $v(X,Z)$ is its velocity directed along the Z-axis. Assuming that the electrons are emitted with zero speed we have $v(X,Z)=\sqrt{2e\Phi(x,z)/m}$ and, therefore, using Eq. (2) the electric potential in the chosen cell satisfies the Poisson equation

$$\frac{\partial^2\Phi}{\partial X^2} + \frac{\partial^2\Phi}{\partial Z^2} = \frac{e}{\epsilon_0}\rho(X,Z) = \sqrt{\frac{m}{2e}}\frac{J(X)}{\epsilon_0\sqrt{\Phi}}, \tag{3}$$

where m is the electron mass and ϵ_0 is the electric constant. The shape of the electrodes is taken to be symmetric about the Z-axis as in Fig. 1 and thus the whole problem is reduced to finding the solution of Eq. (3) in the region between $X=0$, $X=M$ and the curves representing the electrodes: we let $Z=U(X)$ be the shape of the cathode and $Z=W(X)$ that of the anode. The boundary conditions are:

$$\Phi/_C = 0, \quad \Phi/_A = V, \quad \frac{\partial\Phi}{\partial X}(0,Z) = \frac{\partial\Phi}{\partial X}(M,Z) = 0, \tag{4}$$

and one more which relates the emission to the electric field at the cathode,

$$J(X) = F[E_n(X)], \quad \text{where} \quad E_n(X) = \left|\vec{\nabla}\Phi[X,U(X)]\right|. \tag{5}$$

Note that Eq. (5) involves the gradient of Φ, i.e., the electric field E_n normal to the cathode surface. The positive function F defines the law of the field emission. The solution of Eqs. (3)–(5) will yield the potential Φ, ρ, and $J(X)$.

For convenience of computations we introduce dimensionless functions and variables

$$x = X/M, \quad z = Z/L, \quad \varphi = \Phi/V, \quad u(x) = U(X)/L, \tag{6}$$

$$w(x) = W(x)/L, \quad f = E_n/E_0,$$

and denote $E_0=V/L$, $L/M=h$, where L is the maximum distance between the electrodes. Equations (3)–(5), which determine our problem, then can be presented in the form

$$\frac{\partial^2\varphi}{\partial x^2} + \frac{\partial^2\varphi}{h^2\,\partial z^2} = \frac{j(x)}{\sqrt{\varphi}}, \quad 0 \le x,z \le 1,$$

$$\varphi[x,u(x)] = 0, \quad \varphi[x,w(x)] = 1, \tag{7}$$

$$\frac{\partial\varphi}{\partial x}(0,z) = \frac{\partial\varphi}{\partial x}(1,z) = 0, \quad j(x) = \tilde{F}[f(x)].$$

Using Eqs. (6) and (7) the current density in physical units can be expressed as

$$J(X) = \epsilon_0\sqrt{\frac{2e}{m}}\frac{h^2V^{3/2}}{L^2}j(x). \tag{8}$$

The emission law whose mathematical form is introduced in Eq. (5) by the function $F(E_n)$ and given in Eq. (7) by $\tilde{F}[f(x)]$. It can be obtained from Eqs. (5), (6), and (8) via straightforward computations

$$\tilde{F}(f) = (\epsilon_0 h^2)^{-1}\sqrt{\frac{mL}{2eE_0^3}}F(E_0 f), \quad \text{where} \tag{9}$$

$$f(x) = \sqrt{1 + h^2\left(\frac{du}{dx}\right)^2}\frac{\partial\varphi}{\partial z}[x,u(x)].$$

Here $f(x)$ is the dimensionless electric field at the cathode surface which maps onto $E_n(X)$ with the help of the vacuum field E_0 between two parallel planes separated by the distance L when the potential difference between them is V.

We are dealing here with a nonlinear boundary value problem with a nonstandard set up: besides the unknown function Φ the right side of Eq. (3) is either unknown (in the case of unlimited cathode emissivity) or it is defined by the boundary condition in Eq. (5) which involves an unknown normal derivative of Φ. On the other hand, Eq. (5) is an extra

boundary condition in addition to Eq. (4) which makes the problem well posed. Using from now on the new variables one can say that for getting a reliable solution of Eq. (7) we need a very precise approximation of φ because $j(x)$ is expressed for $z>u(x)$ in terms of its second derivatives. To find such an approximate solution we try to capture the main component φ_0 of the potential φ by using a function which describes a gradual transition of the equipotentials from the cathode shape $z=u(x)$, where $\varphi_0=0$, to the anode, $z=w(x)$, where $\varphi_0=1$.

In this spirit an equipotential curve in the cell at a fixed value of φ_0, $(0\le\varphi_0\le 1)$ is approximated by

$$z = f_1(\varphi_0)u(x) + f_2(\varphi_0)w(x), \tag{10}$$

where both f_1 and f_2 are monotonic and satisfy the conditions

$$f_1(0) = f_2(1) = 1, \quad f_1(1) = f_2(0) = 0. \tag{11}$$

Additional conditions on f_1, f_2 are imposed by our requirement that Eq. (10) be invertible. We choose quadratic polynomials for both f_1 and f_2 which, being bounded by Eq. (11), will have only two free parameters c_1, c_2, e.g.,

$$f_1(\varphi_0) = (1-\varphi_0)(1-c_1\varphi_0), \quad f_2(y) = \varphi_0[1-c_2(1-\varphi_0)].$$

This drastically decreases the computational complexity and time by obtaining from Eq. (10) $\varphi_0(x,z)$ in an explicit form. Note that the smoothness and symmetry of $u(x)$, $w(x)$ and the properties of f_1, f_2 make the boundary conditions in Eq. (7) satisfied by the function $\varphi_0(x,z)$ which gives a principal contribution to $f(x)$ and therefore to the cathode current, see Eq. (9).

The strategy of solving Eqs. (7)–(9) is rather straightforward: we supplement the function $\varphi_0(x,z)$ with a set of correction functions and write the potential in the form

$$\varphi(x,z) = \varphi_0(x,z) + \sum_{i=1}^{N} c_{i+2}\varphi_i(x,z), \tag{12}$$

where the first term φ_0 depends on the unknown parameters c_1, c_2 in addition to $c_3, \ldots, c_{N+2}$ from Eq. (12). The functions $\varphi_i(x,z), i\ge 1$ are constructed with the help of $u(x)$, $w(x)$, variables x, z and their powers in such a way to make each of them consistent with the boundary conditions. Their examples are

$$(lx^k - kx^l)[z-u(x)]^m[w(x)-z]^n,$$

$$[z-u(x)]^m/[w(x)-u(x)]^m - [z-u(x)]^n/[w(x)-u(x)]^n.$$

As the result we use only algebraic functions. With this choice the computation was very fast and the precision was acceptable. For an enhanced flexibility a more general class of the correction functions would be necessary in particular when $h\gg 1$ but h in this work never exceeds 2. The current density depends on the parameters c_k via Eqs. (5) and (8) and $\sqrt{\varphi}$. After substituting Eq. (12) into Eq. (7) we get both linear and nonlinear terms in c_k as well as some terms independent of the c's. By grouping all terms of Eq. (7) on the left side we square the result and then consider the problem of minimizing this square in terms of $c_1, c_2, \ldots, c_{N+2}$ on a representative set of points inside the cell shown in Fig. 1. For this we use direct minimization with iterations for handling the nonlinearity.

It is clear that our choice of f_1, f_2 makes in general the dependence of φ_0 on $z-u(x)\ll 1$ linear for z close to $u(x)$. In the case of infinite cathode emissivity, where the potential is known to behave as $z^{4/3}$ near the flat cathode surface (i.e., when $u(x)=0$), the anzatz for φ_0 is modified to capture this property. We use Eqs. (10) and (11) with the same parametrization as before, but substitute $\varphi_0^{3/4}$ instead of φ_0 in Eq. (10). Thus when the algebraic solution of Eq. (10) is given by $\varphi_0(x,z)$, as the first term in Eq. (12) we will substitute the function $\varphi_0^{4/3}(x,z)$ which has the right dependence when $z\approx u(x)$. The current in this case is not defined by $E_n[x,u(x)]$ which is equal to zero but it will be approximated by a set of function as $j(x)=\Sigma c_k g_k(x)$, $k\ge N+3$, where g_k are consistent with our expectations, say $g_k=u^k(x)$. These new parameters c_k will be used for the optimization along with the parameters introduced in Eq. (12). In both cases criteria for the accuracy of the approximation are not only a small value of the functional to be minimized, but also that the current density defined as $j=\sqrt{\varphi}(\varphi_{xx}+h^{-2}\varphi_{yy})$ be practically independent of z in the whole region.

The whole scheme is developed for arbitrary smooth shapes of the electrodes, but we report here the results of calculations made with $h=1$; symmetric $u(x)=a(1-x^2)^2$, $w(x)=1$, and limited $0\le a\le 0.6$. We consider four emission models: infinite cathode emissivity (CL case), the linear, quadratic, and the FN current-field dependences. While the mapping of our results in dimensionless units onto real measurements is shown for the case of unlimited emission in Sec. III we do not do this for the unrealistic models $j(x)=sf(x)$, $j(x)=tf^2(x)$ which are studied for the sake of qualitative illustrations of the leading tendencies of emission from curved cathodes. The FN emission is explored in more detail using physical units in Sec. V. The computations are accurate within a few percents and errors never exceed 10% for the first three models, but the FN emission is more difficult for the mathematical modeling and sometimes errors are higher especially when the current density is small. The infinite emissivity case requires usually a smaller number of the correction functions but we never used more than 25 unknown parameters c_k in all the cases.

III. INFINITE EMISSIVITY RESULTS

The computations in this case are reliable when the maximum height a of the cathode bump does not exceed much of $h/2$. In Fig. 2 we exhibit the current densities at the top and the valley of the cathode, $j(0)$ and $j(1)$, respectively, along with the average current density. The latter is equal to the total current since we have chosen Eq. (6) units in which $M\to 1$

$$j_{av}(a) = \int_0^1 j(x)ds(x), \quad ds(x) = dx\sqrt{1+h^2\left(\frac{du}{dx}\right)^2}, \tag{13}$$

where $ds(x)$ is an element of the cathode surface.

One can see in Fig. 2 that the current density in the valley of the cathode decreases monotonically when a goes

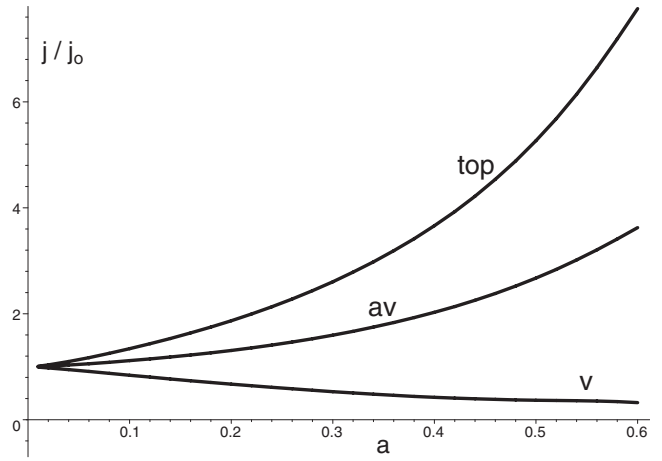

FIG. 2. Plot of current densities vs the cathode bump height a. Top of bump (top) $j(0)$, average (av) j_{av}, and valley (v) $j(1)$ in the CL units $j_0 = 4V^{3/2}/9L^2$.

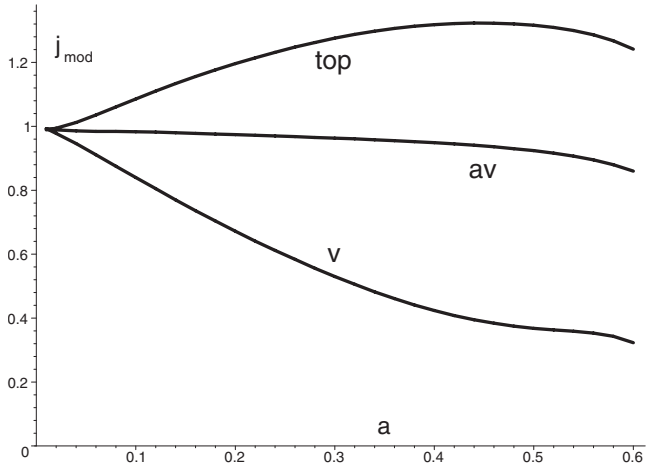

FIG. 3. Current densities modified for the bump shape vs its height a. Curves top, av, and v represent $(1-a)^2 j(0)$, j_m, and $j(1)$, respectively.

up while it grows strongly at the top of the bump but the graphs of $j(0)$ and j_{av} are somewhat misleading because the real interelectrode distance is not the same across the diode while the current density is given in units of j_0 with fixed h. To make the role of cathode curvature more transparent we take into account the varying spacing between the electrodes and modify the current densities by measuring and plotting them in the "local" CL units $j_0[h(x)]$ where $h(x)=h[1-u(x)]$. The mean modified current density is evaluated as

$$j_m = \int_0^1 [1-u(x)]^2 j(x) ds. \tag{14}$$

Figure 3 presents together with $j(1)$ their dependence on a, i.e., plots of $(1-a)^2 j(0)$ and j_m ($j(1)$ clearly does not need the correction). Note that these modified current densities here and below actually are not currents but quantities proportional to them.

Figure 3 shows that the locally normalized top and mean currents do not vary much even when the cathode bump makes the actual distance between the electrodes only 40% of h. Though the electric field tends to be stronger at a curved surface the space charge effects mask this and the current density (measured in corresponding local CL units) levels off after exceeding the 1D CL "limit" by 20%–25%. We may conclude that curving the cathode does not affect the current substantially in the case of the CL emission. Curvature plays however a much more important role in other emission regimes especially in the realistic FN case.

IV. FIELD EMISSION: LINEAR AND QUADRATIC MODELS

Though such emission models, $j_l = sf$, $j_q = tf^2$ with constant s,t, are not realistic, they offer a simple way to study how the curvature of the cathode surface affects the current for different field dependences. We present our results for j_l, j_q in parallel to simplify their comparison. The process here depends on the bump shape, parameter a, and on the values of s or t which characterize the cathode response to the electric field. When $s=t=1$ are fixed and a varies from zero to 0.6, as in Fig. 2, the top current density $j(0)$ increases by a factor ~5 for the linear case and ~8 for quadratic one (these factors are 2.6 and 3.6, respectively, for the average currents j_{av}). In Fig. 4 we show these "currents" after adjusting them to the actual anode-emitter spacing. The linear model is given on the left.

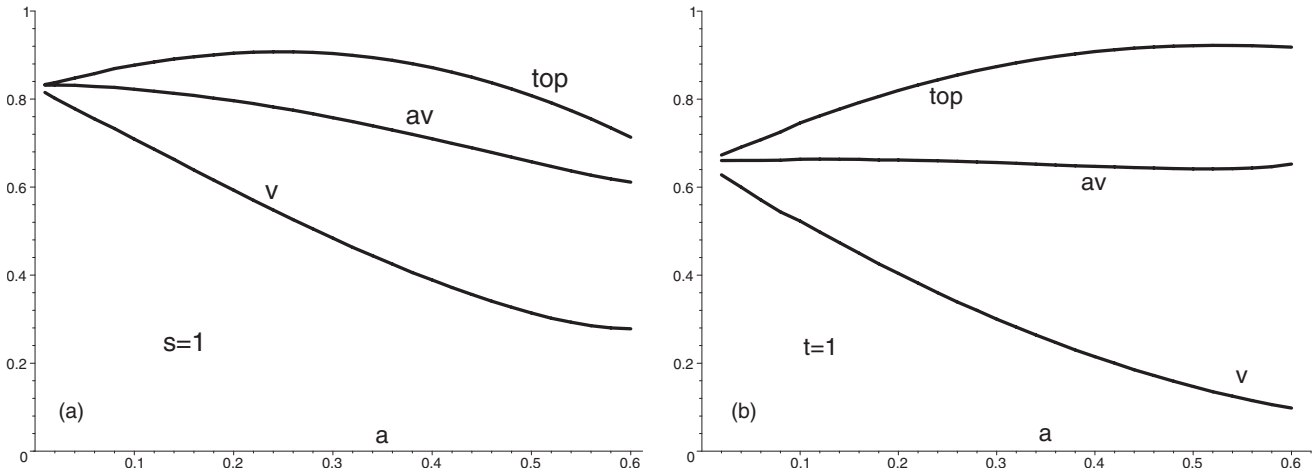

FIG. 4. Current densities normalized to the actual electrode spacing for $s=1$, $t=1$. Curves top, av, and v represent $(1-a)^2 j(0)$, j_{av}, and $j(1)$.

The normalized average current j_{av} is practically stable, the top currents behave rather similarly, but the currents $j_l(1)$ and $j_q(1)$ decrease by factors 2.9 and 6.4, respectively, and thus one might expect that in real situations the contribution from the cathode areas outside of its bump is negligible. Note that the normalized average current

$$j_{av} = \int_0^1 j(x)ds/j_{CL}, \tag{15}$$

is rescaled by the corresponding $j_{CL}(a)$ found for the infinite emissivity case in previous section (j_{av} in Fig. 2). We see that for cathode emissivity $s,t=1$ the top and average currents are not far from the CL limit when $a=0$, but for larger a this $s=1$ is not sufficient and curves for the linear emission go down in Fig. 4. In the quadratic case the top current goes moderately up while j_{av} is almost constant.

The analysis of the graphs in Fig. 4 requires knowledge of the current behavior in the 1D geometry. For example, for the linear model, see Ref. 8, the single parameter, whose growth determines the approach of the current to the CL limit, is $sd/\sqrt{V}$, where d is the interelectrode distance. It becomes smaller when we fix the voltage V and consider the top of the cathode bump. This effect causes the decline of j_l, curve av, in Fig. 4. Note that $j(0)$ is even slightly increasing initially and it decreases less because the electric field becomes stronger faster than d^{-1} when the actual $d(x)$ decreases.

When the cathode emissivity is smaller the starting position of the current density is far from $j_0(1)$ (it corresponds to 1 on the vertical axis), see Figs. 2–4 above, and the increase in the bump height makes all the currents for the linear emission go steadily down in Fig. 5. The more pronounced emission dependence on the field strength in the quadratic case leads to the current growth at the top where the field is stronger. This growth is faster than in Fig. 4 where the space charge is denser.

The dependence of the field emission currents on the parameters of the cathode emissivity s,t when the bump height is fixed, $a=0.3$, are shown in two different forms. We use the local CL (as before) and also the 1D current normalizations. The latter one means measuring the current densities at each x in the units of currents for the 1D system, studied in,[8–10] with the same emission law and the corresponding inter-electrode spacing $d(x)=1-u(x)$.

The current densities in the linear and quadratic cases for the 1D geometry with the anode-cathode distance d and voltage V are found[8] explicitly in the forms, respectively

$$j_l(\alpha)/j_0 = 9\alpha[1+3\alpha^2+(1-3\alpha)\sqrt{1+\alpha^2+2\alpha/3}]/8,$$

$$j_q(\beta)/j_0 = [1+(\beta-1)\sqrt{2\beta+1}]^2/2\beta^3, \tag{16}$$

where $\alpha=sd/\sqrt{V}$, $\beta=2t\sqrt{V}$, and the CL current $j_0=4V^{3/2}/9d^2$. Equations (16) provide at each x the 1D currents densities j_l,j_q in addition to j_0 for constructing the next figures.

The behaviors of current densities shown in Figs. 6 are similar to each other but the approach to the CL limit is slower when the emission is governed by the quadratic law. At small x, where the cathode curvature creates stronger electric fields, the current tends to exceed the CL limit by $\sim$20% in both regimes and this clearly is determined by the cathode curvature which is the same. This effect is expected to be stronger for larger bump heights a. Our chosen $a=0.3$ makes the total currents equal approximately to the CL limit asymptotically, but this will not be so for a different a.

The current in the diode valley, curve v, stays almost constant, but in the linear case it is somewhat lower because the field dependence of emission is sharper. In the linear regime the valley current after reaching $\sim 0.45j_0$ at $s\sim 1$ stays practically independent of s while the total current when $s>3$ is close to the CL current (note that according to Ref. 8 in the 1D case the field emission current needs $s\sim 5$ to reach the same level).

For the whole range of s and t the diode current densities, normalized by the local 1D currents, are almost horizontal, but there is an important feature of the top current in the quadratic regime when t is small and the space charge is tenuous: $j(0)$ (curve v) exceeds the 1D current density by $\sim$50%. Free of space charge electric fields (FSC regime) for $a=0.3$ differ by $\sim$30% and the quadratic dependence on them is sharp enough to make the currents differ by a larger

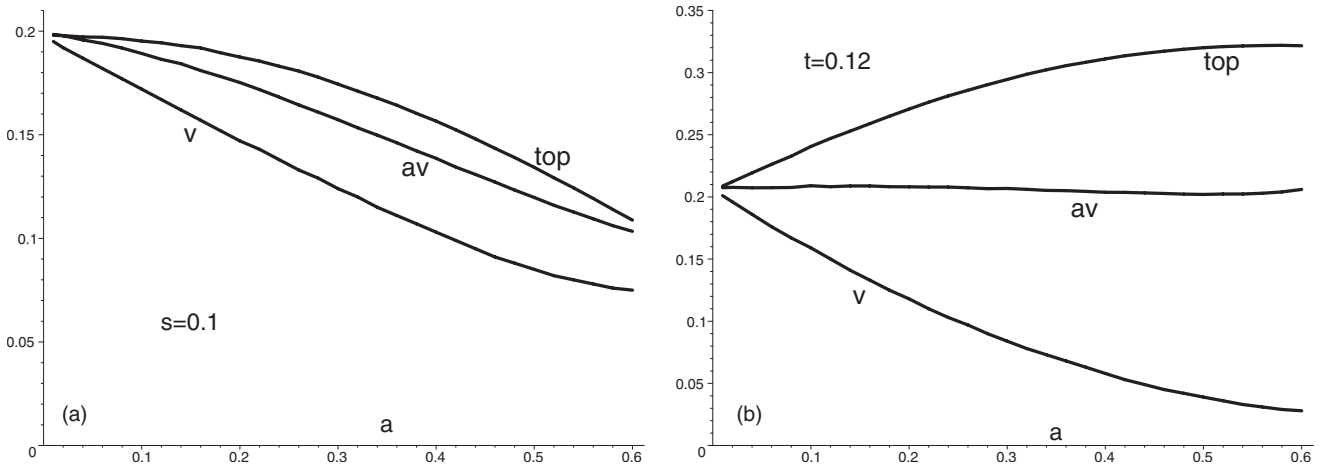

FIG. 5. Current densities normalized to the actual electrode spacing for $s=0.1$, $t=0.12$. Curves top, av, and v represent $(1-a)^2j(0)$, j_{av}, and $j(1)$.

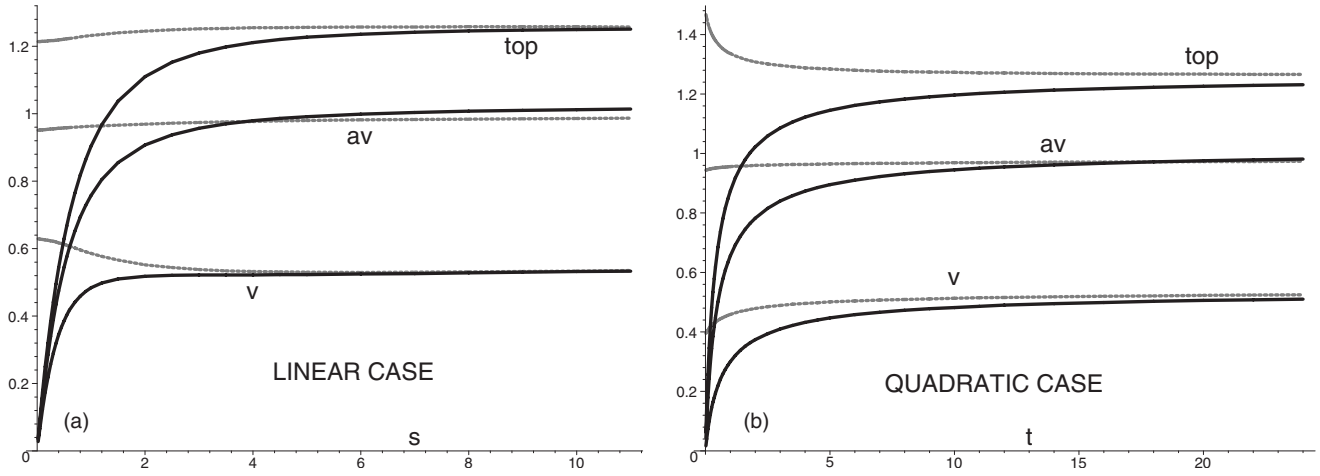

FIG. 6. Current densities vs parameters s and t of cathode response, $a=0.3$. Curves top, av, and v for $j(0)$, j_{av}, and $j(1)$ normalized by local CL (black) and 1D (light) currents.

amount. Our computations did not show this effect in the linear case, but it will be very large in the FN emission regime.

We emphasize the important feature of the graphs in Figs. 6 which exhibit a rather small change in the current ratios when the cathode response to the field (parameter s or t) and, therefore, the current and space charge density increase. Thus the distribution of emission from different cathode points is determined almost solely by the curvature at these points and stays the same, while the current density changes all the way from the FSC to the CL regime.

V. FN EMISSION LAW

The FN emission law with modifications has been studied extensively both theoretically and experimentally. The factors Q,P in Eq. (1) depend on the physical parameters of the cathode material and temperature. One of the widely used simple forms is given in[11] as

$$Q = 1.54 \times 10^{-6}/t^2(y)\chi, \quad P = 6.83 \times 10^7 v_F(y)\chi^{3/2}, \quad (17)$$

where χ is the work function expressed numerically in electron volts. The elliptic functions $t(y)$ and $v_F(y)$ depend on the dimensionless parameter $y=\sqrt{e^3E/4\pi\epsilon_0}/\chi$. In the original FN theory $t(y)=v_F(y)=1$ because the attraction[12] between an electron and metal surface does not affect practically the tunneling probability in weak fields and can be disregarded. The attraction changes the shape of the tunneling barrier, which can be approximately incorporated[13] in Eq. (17) using $t(y)$, $v_F(y)$, and it becomes important in strong electric fields when E approaches and exceeds the ballistic limit $E_b \sim 4\pi\epsilon_0 e^{-3}\chi^2$. This limit corresponds to the situation when the top of the potential barrier (rounded by the image forces) becomes equal to the Fermi level. Parameters $t(y)$, $v_F(y)$ are tabulated in Ref. 13 for $E \leq E_b$ but for our calculations we use a very precise and convenient analytic approximation developed by Forbes[14]

$$t(y) = 1 + y^2(1 - \ln y)/9, \quad v_F(y) = 1 - y^2(1 + \ln y^{-1/3}). \quad (18)$$

If E is taken in volts per centimeter the current density $J(X)$ in Eq. (1) will come out in amperes per square centimeter. We study here two cases for χ_k $(k=1,2)$, which correspond to strong (like in copper, 4.5–5.1 eV) and weaker (cesium, 2.14 eV) binding of electrons, and neglect a weak temperature dependence in (17).

The FN boundary condition $j(x)=\tilde{F}(f)$ for the dimensionless Eq. (7) can be written now in the form

$$j(x) = q_k h^{-2}\sqrt{V} f^2(x)\exp[-p_k L/Vf(x)], \quad (19)$$

where the units for numeric values of V,L are kilovolt and micrometer, respectively. For them Eqs. (8) and (9) yield the dimensionless parameters q_k,p_k, proportional to Q,P, respectively, in Table I.

After solving Eq. (7) subject to boundary condition in Eq. (19) the current density in ampere per centimeter square is evaluated using the following form of Eq. (8)

$$J(X) = 1.66 \times 10^7 \frac{h^2 V^{3/2}}{L^2} j(x), \quad (20)$$

where as in Eq. (17) kilovolt and micron are used for convenience.

Figure 7 presents the current density emitted by a cathode of work function 4.5 eV whose shape is characterized by $a=0.3$ when the voltage V varies between 3 and 44 kV.

Figure 8 shows the current densities for $\chi=2$ eV where one can see that choosing cathode materials with lower work function allows to decrease anode voltage to get the same currents in the same geometry. The mean current density for $V=5$ kV is 0.145, 1.08 and for $V=8.5$ kV it becomes 1.20,

TABLE I. FN current: cathode parameters.

k	χ	q	p
1	4.5	2.06	65.2
2	2.0	4.63	19.3

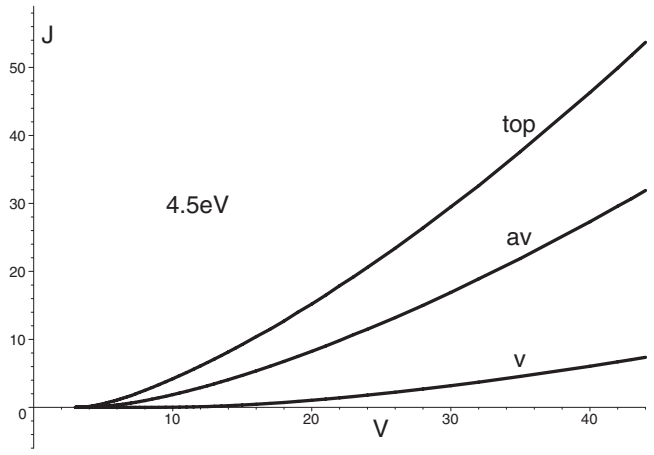

FIG. 7. Top (top), average (av), and valley (v) current densities vs anode voltage The diode parameters are $M=L=1$ μm, $a=0.3$; $\chi=4.5$ eV; V in kilovolt, J in 10^8 A/cm^2.

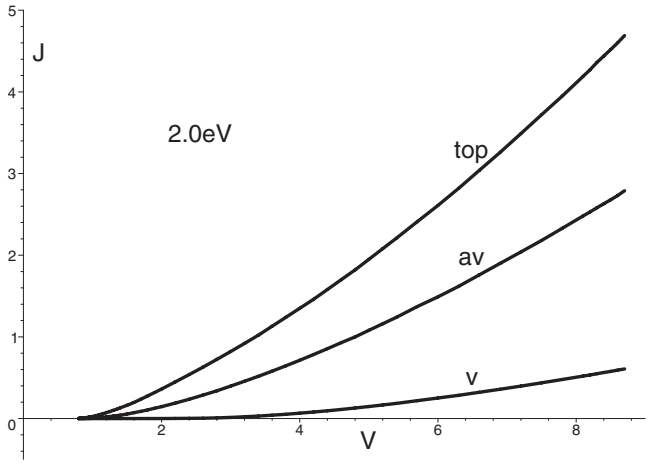

FIG. 8. Top (top), average (av), and valley (v) current densities vs V when $\chi=2$ eV The diode parameters are $M=L=1$ μm, $a=0.3$; V in kilovolt, J in 10^8 A/cm^2.

2.68 when the work function is 4.5 and 2.0, respectively, (the numbers for current density in A/cm^2 should be multiplied by 10^8). In the same time for larger currents one should choose the cathodes with higher work functions because their ballistic field E_b is higher too and they are more tolerant to larger V.

When $E \to E_b$ at the cathode surface our computations become unstable and the precision drops.

It is convenient to use the FN presentation of J, see Refs. 2 and 8, for example, which is suggested by Eq. (1) by plotting the logarithm of J/V^2 versus $1/V$. In the case of a very tenuous space charge the electric field E at the cathode is proportional to V and, therefore, the plot would be a descending straight line. Figure 9, for the same diode parameters as Fig. 7, shows a strong onset of space charge effects when V is sufficiently large, both curves for the top and total currents even go upward. The latter effect was found in Ref. 9 for flat cathodes when the electric field at the maximum of the FN logarithmic plot corresponds to ~ 25 kV/μm while the vacuum field $E_0=V/L$ in Fig. 9 is ~ 10 kV for the top current density. This field, multiplied by the factor $1/(1-a) \approx 1.4$ at the bump apex, is clearly smaller than in the flat case[9] though the space charge is present in both. This is caused by a weaker field dependence of the emission when E approaches to E_b and also a larger value of E at a curved cathode. The average current density (curve av) is similar to one in Ref. 9. The valley current density in Fig. 9 is affected by the space charge only when V is very large (maybe even impossible experimentally) and the graph behavior is approximately linear. The maximum value of this current density is smaller by almost a factor of 10 than the average one while in the cases of linear and quadratic emission laws $j(1)$ is about 1/2 of the average current, see Figs. 2–8. This means that in realistic conditions only a part of the cathode bump near its top produces practically all the current even in our case of a very smooth bump shape and $a=0.3$.

The graphs in Fig. 9 imply that in our system the emitted currents approach the CL limit found[7] for the flat cathodes in 1D geometry. In our set up the current density depends on the cathode curvature and it is higher than the classical one at the curved down cathode surfaces as was seen in Secs. IV and V. Note that the larger current from curved cathodes is caused by both modification of the electric field and by a locally increased emitting area. To get a more descriptive and full picture of our currents we compare them again with the local CL limit and also with the local 1D current. There is no

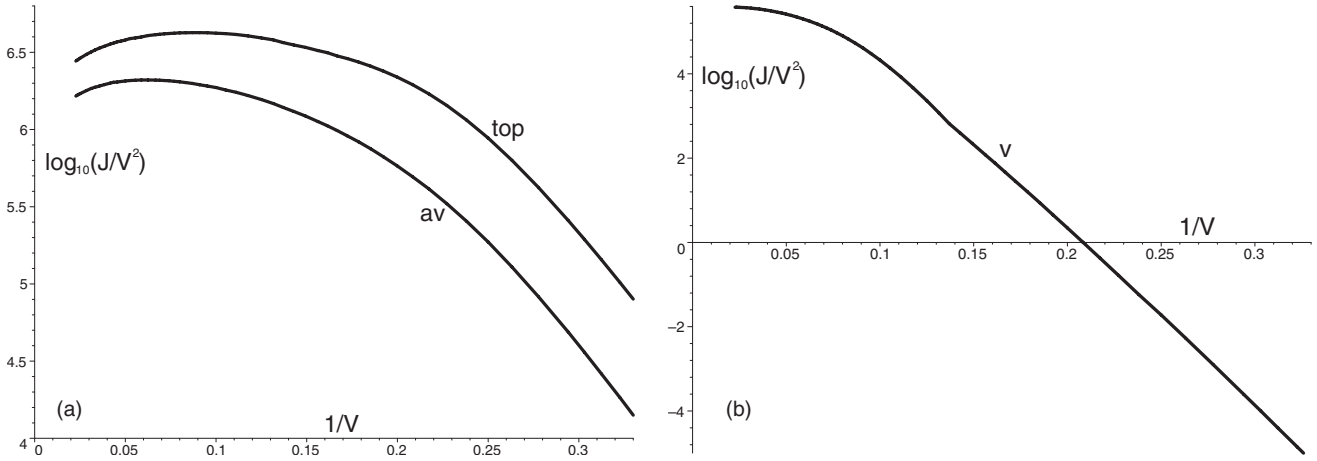

FIG. 9. Plots of $\log_{10}(J/V^2)$ for top, average (av), and valley (v) current densities vs $1/V$ $\chi=4.5$ eV; V in kilovolt, J in ampere per centimeter square.

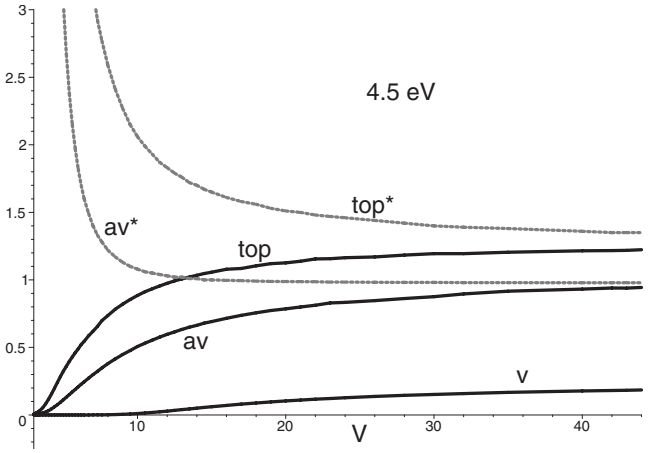

FIG. 10. Plots of normalized current densities vs V (in kilovolt), $\chi=4.5$ eV Curves (top), (av), (v) for $j(0)$, j_{av}, $j(1)$ normalized by CL while (top*), (av*), are 1D normalized $j(0)$ and j_{av}.

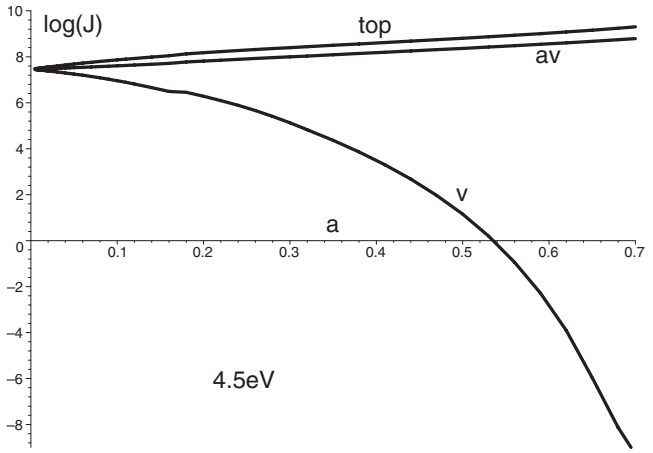

FIG. 11. Plot of current density (ampere per centimeter square) vs the cathode bump height a. Curves (top), (av), (v) represent common log of top, average, and valley currents, respectively.

analytic solutions similar to Eq. (16) for the FN model, but for an arbitrary emission law $F(E)$, including Eq. (1), the 1D current density can be calculated numerically. This requires to come back to the dimensionless Eqs. (7) and use the results of Ref. 8 where we found that this current density can be evaluated by solving for f Eq. (19) together with the following one:

$$j(f) = [2 + (2 - 3f)\sqrt{1 + 3f}]/9, \tag{21}$$

when in Eq. (20) L should be multiplied by $1-u(x)$ at each local point. The solution yields $j(f)=j_1(x)$ which along with the corresponding CL current $j_0(x)$ and the computed solution of Eq. (7) allow us to construct Fig. 10.

The curves in Fig. 10 are constructed in the same way as curves in Figs. 6. The curves $top^*$and av^* are the top and average currents in the local 1D units. We see that curves *top* and top^* asymptotically converge to ~1.25, i.e., 25% above the classical CL limit averaged over the whole emitting area for a diode with the same applied voltage. The average (or total) currents, described by curves *av* and av^*, converge to ~0.95 of the CL limit. The most interesting feature is the behavior of the current density at relatively low anode voltages: when $V=5$ kV the average current exceeds the 1D current by a factor 3, curve av^* while the top current is larger than the corresponding 1D current by a factor of 9 (this is not seen in Fig. 10 where the curves top^*, av^* are cut above $j=3$) and thus provides the main contribution to the average current. This property is absent in the linear field-emission case and only slightly exhibited in the quadratic case. When V increases the electric field at the cathode, screened by the space charge, increases slower than V and the current density approaches to the one emitted by a flat cathode.

The effect of changing the cathode shape, which was studied earlier for simpler emission models, is illustrated here by Fig. 11 devoted again to the case $\chi=4.5$ eV and fixed $V=8$ kV for the diode with $M=L=1$ μm. The sharp dependence of the FN emission on the field strength makes the density of the valley current in Fig. 11 several orders lower and even negligible compared to the top and average currents densities in contrast with Fig. 4 for the linear field emission model where their ratio is only 2 or 3.

We conclude the presentation of the FN emission from curved cathodes by showing in Fig. 12, for the same set of parameters as in Fig. 11, the current densities normalized to the CL and 1D local currents in the spirit of curves shown in Figs. 6.

The *top* current density, top in Fig. 12, is always above 1 while the average one in *av* is close to 1 (comparison with the 1D currents) but the graphs (top, top^*) and (av, av^*), which represent the same current densities, approach each other and their CL limits when the cathode bump grows.

Note that some irregularities in the graphs above, caused by imperfectness of our calculations, are always within a few percent. Insignificant persistent discrepancies between the average currents, say curve *av* in Fig. 6, might be caused by ambiguity in defining averages in different conditions. Our computations for the work function $\chi=2.0$ eV and also for the not very realistic $\chi=0.5$ eV give similar results to those shown here but with lower maximal voltages and currents (we always monitored the electric field at the cathode surface and never exceeded the local values of E_b).

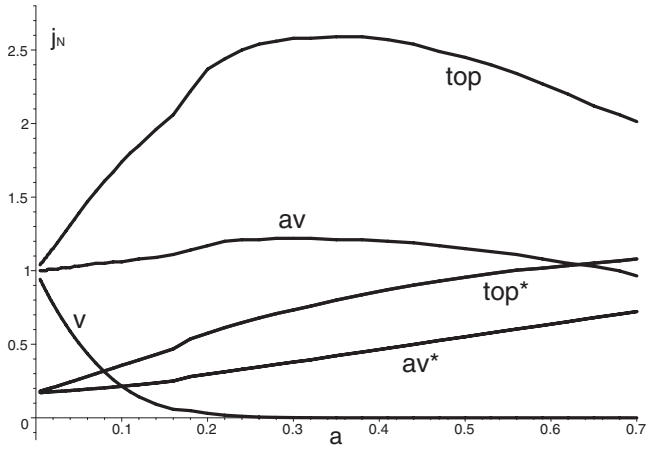

FIG. 12. Plot of normalized FN current densities j_N vs parameter a: top, average (av), and valley (v) in local 1D units; top (top*) and average (av*) in local CL units.

VI. SUMMARY

We studied the effect of curvature of the cathodes on the emitted currents for different field-current emission laws. We considered here the case when the unit of our periodic structure has the same width W and height L, the anode is flat while the cathode has a bump of a smooth analytic shape. Our computation scheme was applied also for more general aspect ratio of the unit and it allows to study curved anodes too. When $M>L$ the precision of the calculations is better and for $M<L<2W$ it is acceptable but we do not report these here. Our results are:

1. In the case of infinite emissivity, which can be a relevant description of the thermionic cathodes, the cathode curvature only slightly affects the maximum and average currents compared with the flat cathode at a corresponding distance from the anode.
2. The dominance of the emission from the most curved area of the cathode gets stronger when the emission dependence on the field strength is sharper: from the linear to quadratic and then to the FN law. The emission from the cathode valley almost disappears in the latter case when the bump reaches 35%–40% of the diode height. The dominant part of the FN current of real cathodes comes from the bump tops, where the curvature is maximal, even when the bump shape is quite smooth. For all current-field laws the spatial pattern of emission is determined by the cathode curvature and depends much less on the voltage V.
3. For a fixed emission model the increase in the cathode parameter (s or t), which determines its response to the field strength, is such that the maximum current density can noticeably exceed the CL limit. We expect this effect to be stronger for cathode shapes with sharp spikes instead of our smooth bumps (which made possible the present computation). The explanation of this surprising property is straightforward: compared with a flat cathode, where the 1D space charge screens the cathode homogeneously, the magnetic field in our case makes the electrons flow in the z-direction without spreading. This yields a column of the space charge, which is dense above the bump top but tenuous around the column. Thus the electric field reaches the cathode better and increases the emission. This effect is stronger in the FN case, where the space charge concentration is larger. Without the magnetic field one can get this effect too because though the space charge is spread out it becomes more diluted in general and does not provide the same screening as in 1D case.
4. The development of experimental techniques can make accessible such strong electric fields that the FN approximation cannot be used. This situation might exist even presently for the electron emission from the tips of very sharp cathode spikes.

ACKNOWLEDGMENTS

Encouragement and comments of R. Barker as well as useful discussions with K. Jensen are greatly appreciated. We also thank the anonymous referee whose attention to our work, comments, and suggestions helped us to improve this paper significantly. Research supported by AFOSR under Grant No. F49620-01-0154.

[1] R. H. Fowler and L. W. Nordheim, Proc. R. Soc. London, Ser. A **119**, 173 (1928).
[2] T. E. Stern, B. S. Gossling, and R. H. Fowler, Proc. R. Soc. London, Ser. A **124**, 699 (1929).
[3] W. Zhu, *Vacuum Microelectronics* (Wiley, New York, 2001).
[4] W. P. Dyke and J. Trolan, Phys. Rev. **89**, 799 (1953).
[5] E. L. Murphy and R. H. Good, Phys. Rev. **102**, 1464 (1956).
[6] R. J. Umstattd and J. W. Luginsland, Phys. Rev. Lett. **87**, 145002 (2001).
[7] C. D. Child, Phys. Rev. **32**, 492 (1911); I. Langmuir, *ibid.* **2**, 450 (1913).
[8] A. Rokhlenko, K. L. Jensen, and J. L. Lebowitz, to appear in JAP.
[9] R. G. Forbes, J. Appl. Phys. **104**, 084303 (2008).
[10] J. R. Barbour, W. Dolan, J. Trolan, E. Martin, and W. P. Dyke, Phys. Rev. **92**, 45 (1953).
[11] R. H. Good and E. W. Müller, *Handbuch der Physik* (Springer-Verlag, Berlin, 1956), p. 176.
[12] W. Schottky, Phys. Z. **15**, 872 (1914).
[13] R. E. Burgess, H. Kroemer, and J. M. Houston, Phys. Rev. **90**, 515 (1953).
[14] R. G. Forbes, J. Appl. Phys. **89**, 113122 (2006).